6

Canonical Examples

6.1 Introduction

This chapter presents the modeling of a variety of simple waveguide, filter and antenna examples. The models can be easily understood from basic theory or there are known solutions, either in mathematically closed form from standard literature or as simulation or measurement results from reliable literature sources.

The examples serve two purposes. First, the reader gets a short tour through some *real* simulations, i.e., the simulations have been performed using up-to-date commercial field solvers. Second, the examples are *useful starting points* for the reader to gain own simulation experience. The advantage with the simple examples is that they result in small simulation models that can be solved within minutes. This may encourage the reader to test different modeling approaches to become familiar with the software.

This book is not intended as a tutorial explaining the GUI structure or praising special features of particular software packages. To avoid benchmarking of different numerical techniques and software packages we have not shown explicit simulation times. Commercial simulation software is subject to constant development and computer speed is increasing rapidly. The aim of this chapter is to work out some important modeling techniques and to consolidate the understanding of the different numerical methods without getting lost in too much details. The reader can apply the examples to the software package used or evaluated.

6.2 Coaxial Line Discontinuity

6.2.1 Theoretical Background

Transmission lines are used to guide electromagnetic energy from a source to a load. The energy transport is realized by a propagating wave on the line. If the line is homogeneous (the cross-section does not change with longitudinal coordinate) and consists of two conducting lossless wires in a uniform lossless medium, the fundamental mode of propagation is the TEM wave mode as discussed in Sect. 2.10. The transmission line can be characterized by its line impedance Z_0. If the cross-section changes abruptly, a reflected wave occurs at the discontinuity due to the disturbance of the TEM field pattern. The reflection coefficient can be determined from the line impedances of the two lines.

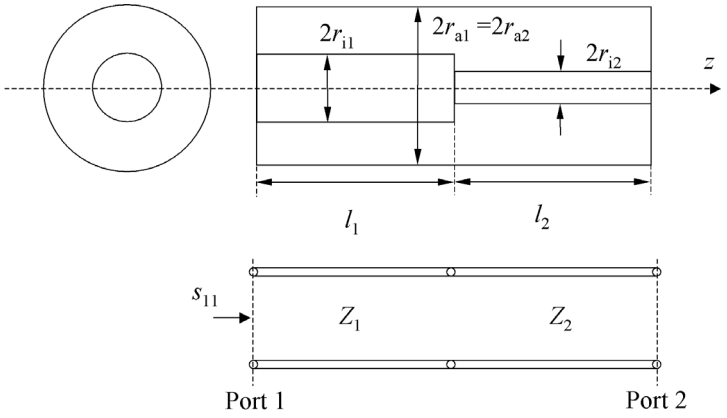

Fig. 6.1. Coaxial transmission line discontinuity

Figure 6.1 shows a transmission line discontinuity where two coaxial lines with different line impedances Z_1 and Z_2 are connected. The geometrical and dielectric properties of the lines are

- outer radius $r_{a1} = r_{a2} = 1$ mm
- inner radius $r_{i1} = 0.3$ mm
- inner radius $r_{i2} = 0.090385$ mm
- length $l_1 = 1.5$ mm
- length $l_2 = 1.5$ mm
- relative permittivity $\varepsilon_r = 2.08$
- loss tangent $\tan\delta = 0$

From the geometric data of the lines and the dielectric properties of the material within the line we can calculate the line impedances from the following equation

$$Z = \frac{60\,\Omega}{\sqrt{\varepsilon_r}} \ln\left(\frac{r_\mathrm{a}}{r_\mathrm{i}}\right) \tag{6.1}$$

as $Z_1 = 50\,\Omega$ and $Z_2 = 100\,\Omega$. The amplitude of the reflection coefficient for a wave travelling in positive z-direction is

$$|s_{11}| = \frac{Z_2 - Z_1}{Z_2 + Z_1} = \frac{1}{3} \quad . \tag{6.2}$$

Since the transmission line is lossless the amplitude of the transmission coefficient is determined by

$$|s_{11}|^2 + |s_{21}|^2 = 1 \tag{6.3}$$

which gives a value of $|s_{21}| = 0.9428$ for the transmission coefficient. The phase angles of the scattering parameters depend on the locations where ports are defined. For example, the phase angle φ_0 (in rad) of s_{21} decreases linearly with frequency and distance between the ports:

$$\begin{aligned} \varphi_0 &= -kl = -\frac{2\pi}{\lambda}\,(l_1 + l_2) \\ &= -\frac{2\pi f}{c_0}\,(l_1 + l_2)\,\sqrt{\varepsilon_r} \quad . \end{aligned} \tag{6.4}$$

In the following subsections we investigate this structure with FDTD and FEM software in the frequency range from 5−25 GHz.

6.2.2 Analysis with FDTD Software

The construction of the Finite-Difference Time-Domain[1] model for a coaxial transition according to Fig. 6.1 starts with the definition of a metallic (PEC) block as shown in Fig. 6.2a. From this block a cylinder with radius r_{a1} is subtracted. In this cylindrical hole two PEC cylinders are placed that represent the inner conductors (Fig. 6.2b). The background material, i.e., the material property of the regions where no objects are placed, has been defined as dielectric material ($\varepsilon_r = 2.08$). The resulting geometrical model is shown in Fig. 6.3. To show the inner structure of the model a part of the geometry is hidden and depicted by a wire-frame representation.

At the outer surfaces of the computational domain perfect electric boundaries are applied. At the top (at z_max) and bottom (at z_min) surfaces of the structure two TEM waveguide ports are defined that represent matched, semi-infinite transmission lines. Figure 6.4 shows the electric and magnetic field

[1] *Microwave Studio* from CST [14]. The software package *Microwave Studio* is based on Finite Integration Technique. As mentioned in Sect. 4.5 in the time-domain the FIT approaches the FDTD method. Since the simulations we show here apply the transient solver of the software, the models and results are presented under the 'FDTD' label.

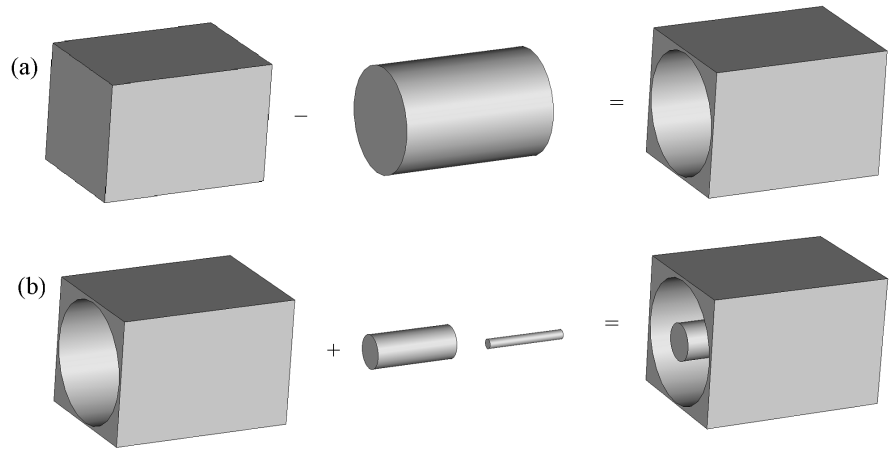

Fig. 6.2. Steps for constructing the geometry of the coaxial line transition: **(a)** a cylinder is subtracted from a metallic box to create a cylindrical hole and **(b)** two metallic cylinders are placed within the cylindrical hole to represent the inner conductors

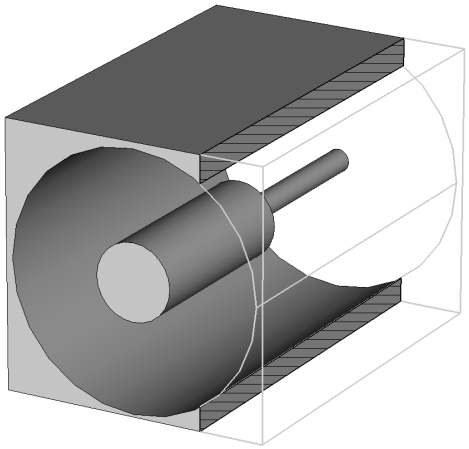

Fig. 6.3. Geometry of the coaxial line transition

strengths at port 1. As already shown in Sect. 2.10 the electric field **E** points radially from the inner to the outer conductor and the magnetic field **H** circulates in azimuthal direction.

The mesh is generated automatically by the mesh generator. Since the geometrical features of the model are small compared to wavelength, the cell size is determined by the geometry. The number of cells is $N = 50 \times 50 \times 40 =$

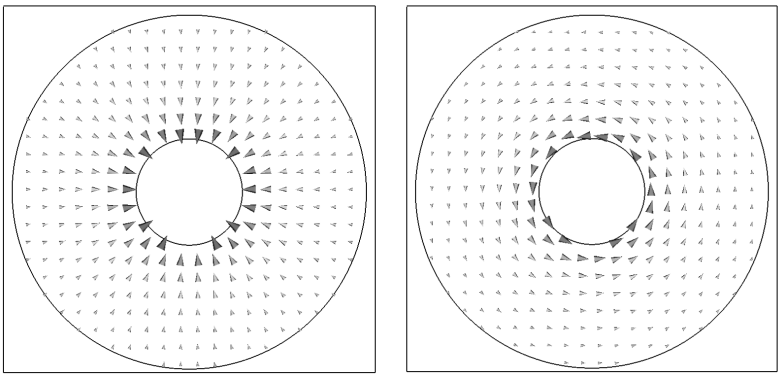

Fig. 6.4. TEM port modes: **(a)** radial electric field strength **E** and **(b)** azimuthal magnetic field strength **H**

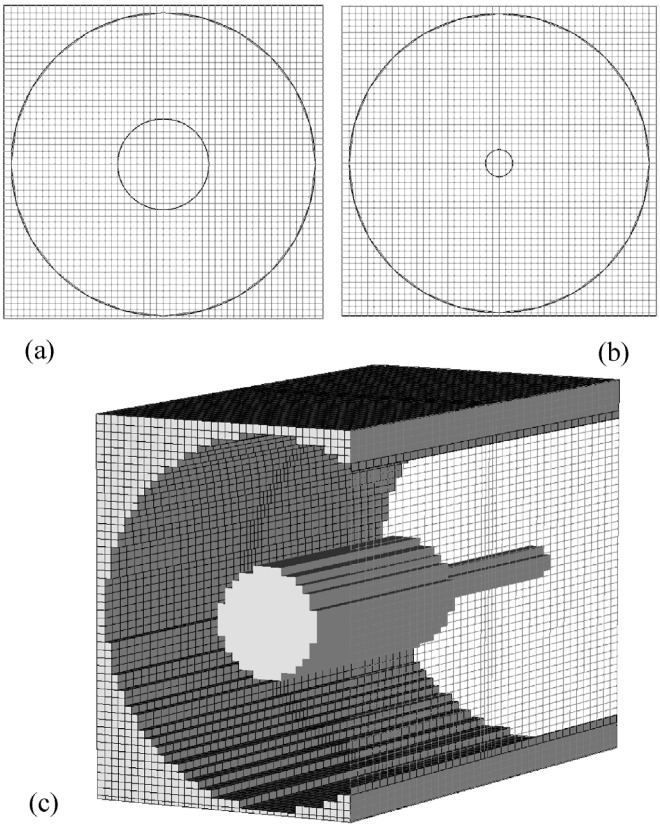

Fig. 6.5. FDTD staircase mesh: **(a)** area at port 1, **(b)** area at port 2, and **(c)** perspective view (a part of the structure is transparent to show the inner conductors)

100 000. Figure 6.5 shows the resulting orthogonal mesh at the two ports and in an additional perspective view.

Since in FDTD a broadband pulse signal may be used, only a single simulation is required to obtain results in the complete frequency range. The frequency-domain response of the structure is obtained by Fourier transforming the time-domain signal response (see Sect. 4.2.6).

In order to calculate s-parameters in the frequency range from 5−25 GHz a Gaussian pulse with a center frequency of 15 GHz and a half-bandwidth of 10 GHz can be used. The time-domain solution process ends after the electromagnetic energy in the computational volume is sufficiently decayed (typically at least −30 dB). The time step is $\Delta t = 5.94 \cdot 10^{-14}$. The number of simulated time steps is $n = 6\,102$. The simulation takes only a few minutes on a standard PC. Figure 6.6 shows the incoming excitation signal (i1) at port 1, the outgoing time signal (o2) at port 2, and the reflected time signal (o1) at port 1. For non-resonating, electrically small structures, like the coaxial discontinuity in this section, the duration of the simulation is mainly determined by the length of the excitation signal.

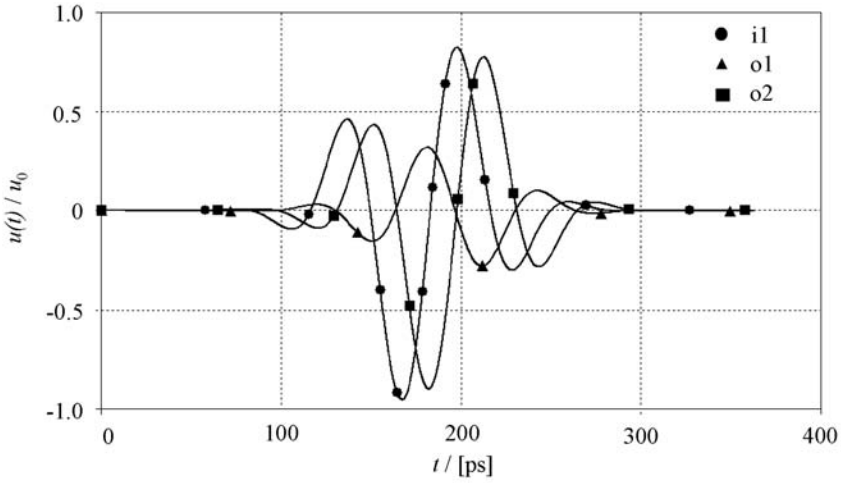

Fig. 6.6. Time-domain signals (frequency range 5−25 GHz): Incoming voltage wave (i1) and outgoing voltage wave (o1) at port 1 and outgoing voltage wave (o2) at port 2

Although the frequency content of the excitation signal discussed above is sufficient for the required s-parameter response the simulation time can be shortened by using an excitation signal that covers a wider frequency range. Figure 6.7a shows the time-domain excitation signal with a center frequency of 0 Hz and a half-bandwidth of 30 GHz. This larger bandwidth leads to a shorter excitation signal and time response. Now only $n = 2\,068$ time steps

are required. This is a significant reduction compared to the first simulation with limited bandwidth.

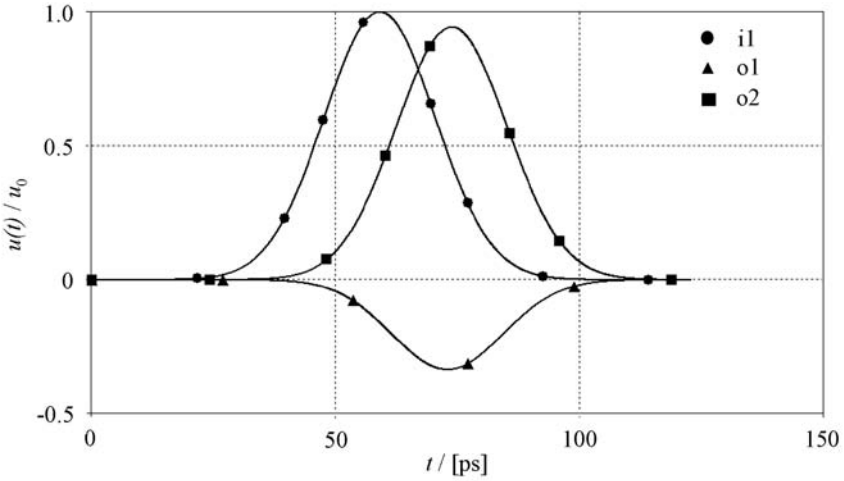

(a) Time-domain voltage signals at the ports

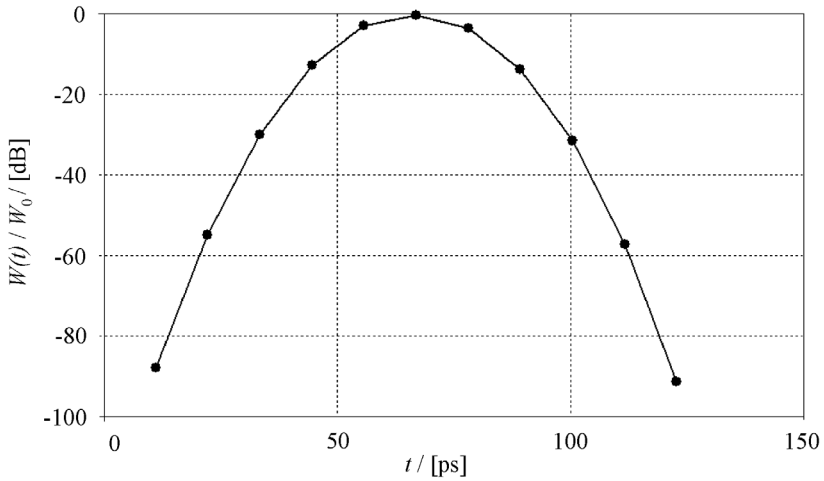

(b) Energy inside the computational volume as a function of time

Fig. 6.7. Time-domain signals ((frequency range 0−30 GHz)): **(a)** Incoming voltage wave (i1) and outgoing voltage wave (o1) at port 1 and outgoing voltage wave (o2) at port 2 and **(b)** energy in the computational domain as a function of time

Figure 6.8 shows the resulting s-parameters in the frequency range from 5−25 GHz. The results match perfectly with the expected values: $|s_{11}| = |s_{22}| = 0.333$ and $|s_{12}| = |s_{21}| = 0.943$. According to Equation 6.4 for a

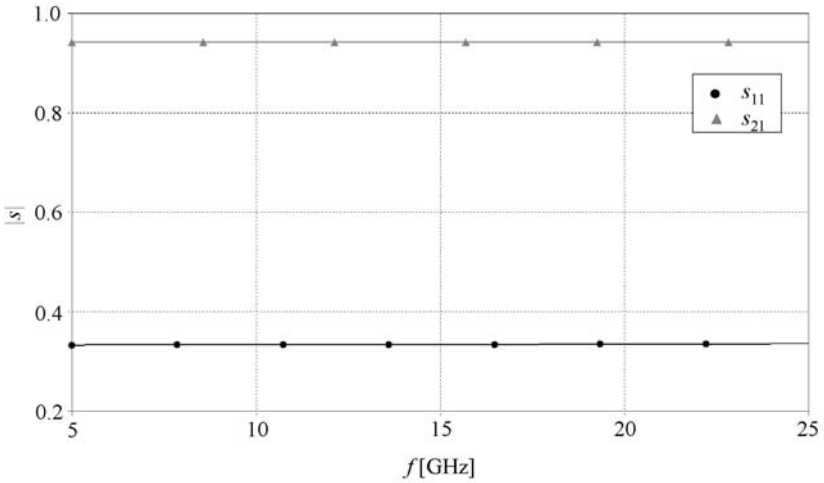

(a) Magnitude of s-parameters s_{11} and s_{21}

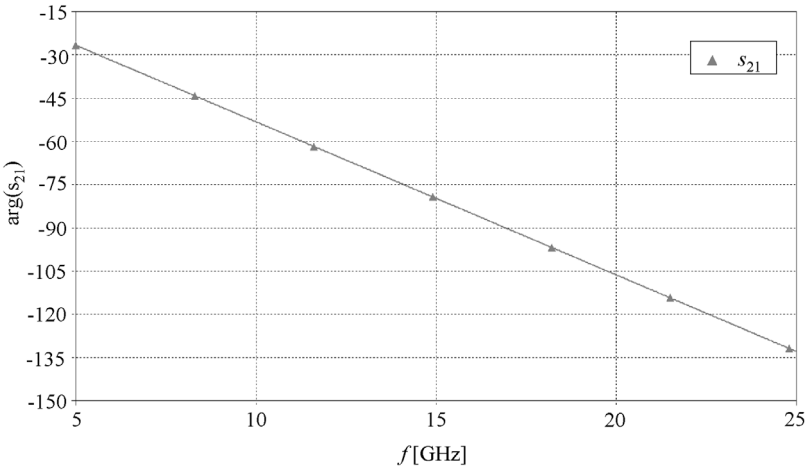

(b) Phase of transmission coefficient s_{21}

Fig. 6.8. S-parameter results for the coaxial line transition: **(a)** magnitude of s_{11} and s_{21} and **(b)** phase of s_{21}

frequency of $f = 20$ GHz we expect a phase angle of $\varphi_0 = -104°$. The simulation result for the phase angle is $\varphi_0 = -106°$ which is in good agreement with theory.

7.4 Ultra-Wideband Antenna Design

7.4.1 Introduction

Currently, PANs (Personal Area Networks) employ wired and unwired links. While the link between the modem and the laptop computer is nowadays typically achieved by WLAN (Wireless Local Area Network) and the connection between the laptop and the printer works also unwired by Bluetooth, high data rate links, e.g., the transmission of the video signal between the DVD player and the flat screen is still established as a wired connection. It is the idea of major companies working in the definition and the design of consumer applications to unwire any wired connection, even the high data rate video links. Such a concept could be called wireless USB (Universal Serial Bus) similar to the well-established wired USB interconnections. An interesting prospective on systems and applications is given in [34]. Especially for high data rate links *Ultra-WideBand* (UWB) systems become very appealing since the FCC opened the spectrum from 3.1 GHz to 10.6 GHz for the unlicensed low-power use [16] [60]. As any other complex RF-system that has to be introduced in

Fig. 7.58. Different home entertainment systems are connected via UWB links

the market within a short time frame, the design of UWB systems requires numerical simulations of different implementations at an early stage, because prototypes are not yet available. For UWB systems, the demands for the antenna are often not limited to large bandwidths only. Other quality criteria,

like low ringing and gain stability over the frequency range, are often required [60] and are, of course, influenced by the specific implementation of the antenna in the user environment. Furthermore, in many cases it is not sufficient to describe the necessary antenna performance of the RF-device by such simple antenna measures only. When the link quality between different systems in a realistic environment is evaluated other aspects like fading, multipath and absorption have to be considered. This procedure leads to propagation modeling and therefore requires the use of other simulation programs which use the prior assessed antenna characteristics.

Figure 7.58 shows a photograph of a living-room having different home entertainment systems, which are interconnected via ultra-wideband links, as an example for the entire scenario to be investigated. In this section we present a method for the efficient characterization of UWB antennas including their specific integration scenario in a device of a home entertainment system by numerical simulations. It shows the complete process beginning with the design and optimization of a broadband antenna element. Then the antenna element is integrated into a realistic model of a home entertainment device and the influence of the integration on the antenna characteristics is investigated. Finally, we show how to extract the results from the field simulation for the later use in propagation modeling. Especially the last step gives an impression how an interface between different modeling techniques can be established.

7.4.2 UWB Antenna Element Design and Optimization

From the EM modeling point of view a suitable antenna element itself has to be designed in the first step. Due to the intended application the following basic requirements for the antenna element can be listed:

- Large bandwidth (e.g.: $s_{11} \leq -10\,\mathrm{dB} \quad \forall \quad f \in [3.1\,\mathrm{GHz}, 10.6\,\mathrm{GHz}]$),
- small size (integration into device),
- low cost technology.

Browsing recent antenna literature a broadband planar monopole antenna is a good candidate. The antenna shape differs from a basic wire monopole in the way that the element provides a smooth taper relative to the groundplane. By optimizing this taper, broadband impedance matching can be obtained quite simply. Figure 7.59 shows some examples of basic shapes for planar broadband monopoles.

Before starting the design and optimization of the antenna element we have to choose an appropriate numerical method which is best suited to solve the problem. By referring to our general catalogue in Sect. 5.11 we notice first that it is likely that there will be arbitrarily shaped objects to be modeled. This gives credit to methods like Method of Moments (MoM) or Finite Element Method (FEM) and will be a drawback for the Finite-Difference Time-Domain method (FDTD) due to the orthogonal grid. As it is best to model the antenna

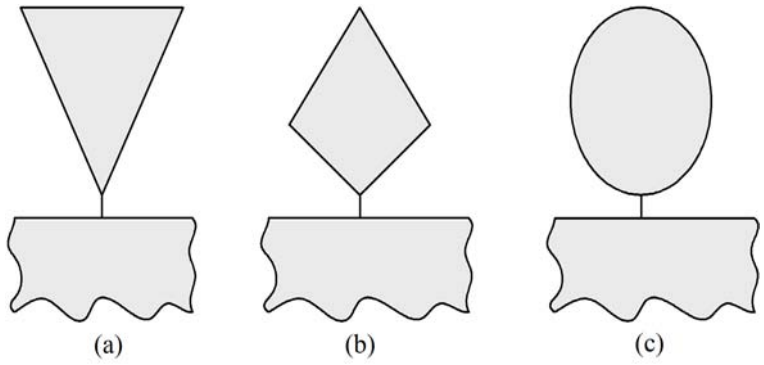

Fig. 7.59. Different basic shapes of planar broadband monopoles on a groundplane

being a planar metallization on a thin sheet of substrate, e.g., a Printed Circuit Board (PCB), the numerical method has to be capable of treating different homogeneous material distributions. This brings credit to FEM and may also be capable for MoM. But, the most evident point to be considered is the fact that we will have to compute a large frequency range. This will result in a large number of simulations for a frequency-domain method, but will bring credit to a time-domain method. Therefore we choose the FDTD method to model this problem and we will see how to cope with staircasing due to the orthogonal grid. The commercial simulator used for his study is *EMPIRE*[14].

The antenna is designed as a planar metallization on a *Teflon* substrate. Such materials are widely available and commonly in use. For instance the material *Rogers RO3003* is available with a thickness of 800 μm. The dielectric constant is $\varepsilon_r = 3.2$. The dielectric losses are moderate. For the numerical simulation we consider the material to be lossless. The substrate is available with a metallization thickness of 17 μm. For the simulation we model the metallization to be an infinitely thin perfect conductor. This will reduce the computational effort, as it is shown in Chapter 5. It is planned to mount the antenna perpendicularly on the PCB of the UWB module in the device. At this modeling step we consider the antenna to be mounted on a groundplane by using an electric boundary in the simulation.

Figure 7.60 shows the model of the antenna in the computational domain. The size of the substrate is 20 mm by 25 mm. The antenna is attached to the bottom boundary which is defined to be an electric boundary. This is a perfect representation of a groundplane, on the one hand, and reduces the computational effort due to the simple definition of the field at this boundary. All other boundaries are modeled to be PML absorbing boundaries (6 layers) in order the provide a free space continuation of the computational domain to the antenna. The distance of the antenna to the boundaries is set to be

[14] *EMPIRE* from IMST [33]

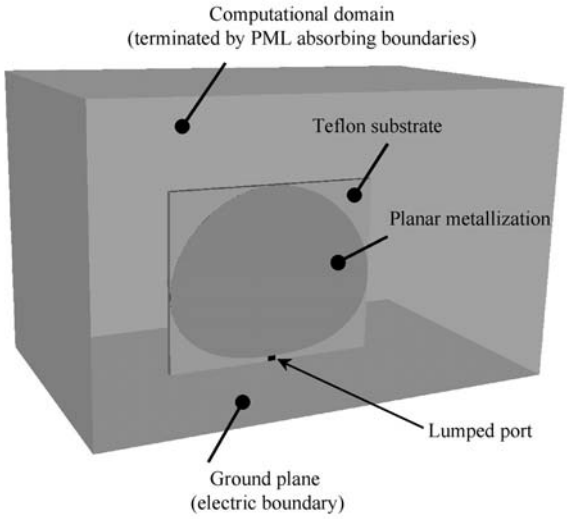

Fig. 7.60. Simulation model in the FDTD computational area

around 15 mm at each side. This corresponds to approximately $\lambda/6$ at the lowest frequency of interest ($f = 3\,\mathrm{GHz}$). Based on the knowledge we have from the basic models investigated in the prior chapters this value should be fine.

The present example is ideally suited to investigate the influence of different dense discretizations of the computational domain. If we just apply the $\lambda/10$ rule in order to minimize numerical dispersion (as discussed in Chapter 5) the maximum cell size can be approximately 3 mm. Due to the orthogonal grid the curved shape of the monopole is represented by a staircased approximation. Depending on the distance of the gridlines the staircasing is be more coarse or dense. Figure 7.61 shows the result of three different discretizations of the curved monopole shape. Figure 7.61a uses a homogeneous grid of 1 mm spacing. It is clearly visible that the resolution of the structure is very coarse in this case and it is likely that the results are clearly dependent on the staircasing in this case. In order to investigate this effect a second model with a homogeneous discretization in the area of the antenna of 0.25 mm is created. Figure 7.61b shows that this results in a much more detailed representation of the curved structure.

While the simulation time increases by a factor of five from the model in Figure 7.61a to the model in Fig. 7.61b the results differ quite small. Trying different inhomogeneous discretizations it can be found that we only need dense spatial resolution in the lower part of the monopole. Figure 7.61c shows the staircased structure for an inhomogeneous discretization rising from 0.25 mm at the lower part to 1 mm at the outer part of the monopole in the different dimensions. The simulation time is only increased by a factor of two

compared to the model in Fig. 7.61a while the results are quite close to the overall dense model. Furthermore, using a maximum cell size of 1 mm also in the outer region of the computational domain allows us to use a maximum frequency of the excitation pulse of 30 GHz. Even if we are only interested in frequency-domain results of up to 11 GHz, it is advantageous to use a broadband excitation pulse, because it is short in the time-domain, and thus reduces the simulation time.

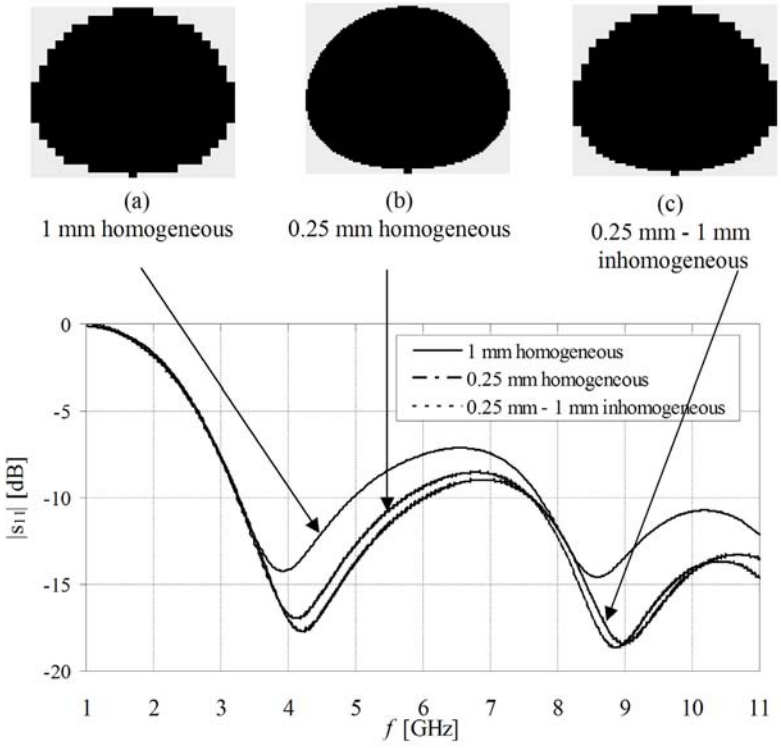

Fig. 7.61. Effect of different dense discretization on the antenna matching

As mentioned at the beginning of the section the matching can be optimized by modifying the taper of the antenna. In order to apply an automatic optimization process, as it becomes more and more available in state-of-the-art simulation software, it is advantageous to describe the antenna by an analytic mathematical function. This function can be, for example, polynomial, elliptical, exponential or any other kind of analytical function which provides a smooth taper. The antenna in Fig. 7.62 is defined by a polynomial function as follows:

$$x = \frac{w}{2} \sin(\pi\alpha) \tag{7.7}$$

$$y = \frac{h}{2} \cos(\pi(k\,|\alpha|^{p_1} - 1)) \quad . \tag{7.8}$$

While w is the maximum width of the antenna and h is its maximum height the parameter α ranges within $-1 \leq \alpha \leq 1$. In Eq. 7.8 the factor k is

$$k = \frac{\arccos(2p_2 - 1)}{\pi} + 1 \quad . \tag{7.9}$$

These continuous Euclidean functions depend on the parameter p_1 (as shown in Fig. 7.62a) and the parameter p_2 (as shown in Fig. 7.62b), which enable a continuous transition into manifold antenna shapes (circle, ellipse, triangle-like, $\cdots$).

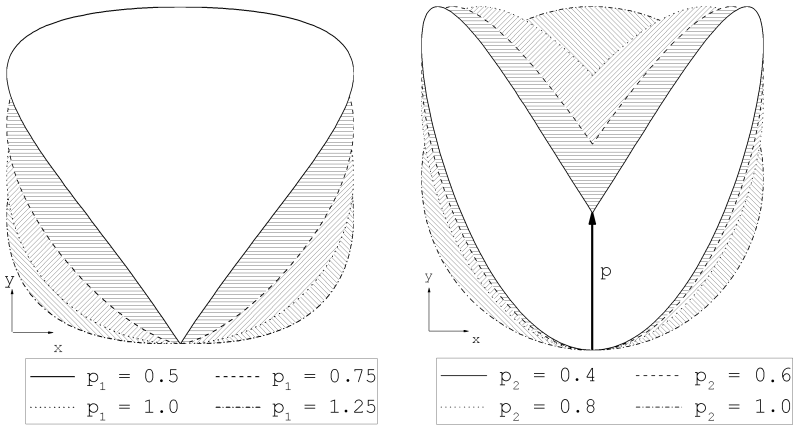

(a) Variation of p_1 **(b)** Variation of p_2

Fig. 7.62. Parametric generation of various shapes

The shape of the antenna is now defined as a parametric object in the CAD-based Graphical User Interface (GUI) of the simulation software. All variables in Eqs. 7.7 and 7.8 can now be assessed by the defined parameters. This provides an easy way to generate a large number of different shapes for a series of simulations or the use of an optimizer. When an optimizer is available within the simulation software, different variations are generated automatically and varied in order to approximate a certain target function which has to be defined in advance. For our example the target function could be:

$$\text{target}(p_1, p_2, \ldots) = s_{11} \leq -10\,\text{dB} \quad \forall \quad f \in [3.1\,\text{GHz}, 10.6\,\text{GHz}] \tag{7.10}$$

Starting from a certain initial state the parameters are now varied and after each step the approximation of the simulation result to the target function is evaluated. The next evolution of the shape is now chosen on the basis of an estimation by a gradient approach or a genetic algorithm, depending on the optimizer. Figure 7.63 shows the results of two different shapes that fulfill the target function in comparison to the initial design of the monopole.

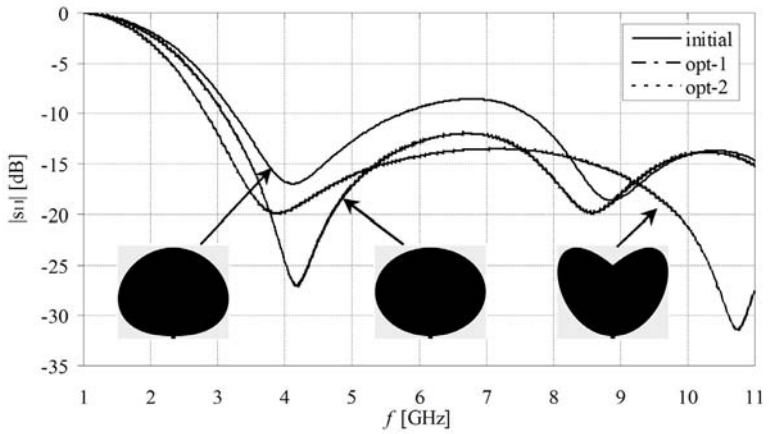

Fig. 7.63. Results from the parametric optimization

Based on the above results it seems that an optimizer may be some kind of holy grail for the numerical design of components. We only need to define a parametric structure and everything else is done by the machine over night. This is usually not the case. Without a good starting structure, a careful definition of the target function, and a sufficient portion of physical insight into the structure we would result in thousands of simulations providing not even one good result. Even when computers become faster and faster the engineer should use an optimizer for what it is made for - optimization of already quite good structures by only slight variation of a small number of parameters.

7.4.3 The Influence of a Specific Integration Scenario

In most cases an antenna is not designed to operate in a free space environment. In this respect the above designed broadband monopole is intended for the integration into devices of home entertainment systems, e.g., a DVD player. It is obvious that the specific integration scenario will have an influence on a radiating component like an antenna. Nevertheless, the basic design in an artificial free space environment makes sense in order to have a good starting value of the component parameters.

In this paragraph we will integrate the prior designed broadband monopole into a numerical model of a DVD player and investigate the influence of the specific integration scenario on the antenna performance.

When an antenna is integrated into a consumer application, other quality criteria than only technical aspects become very important. In this sense the antenna should be completely integrated into the device in order not to disturb the aesthetic design by an extruding antenna. The space occupied by the antenna should be as small as possible. Nevertheless, it is obvious that the antenna requires a certain volume of free space around the radiating component.

Figure 7.64 shows an example of the intended integration scenario of the broadband monopole into a DVD player. The antenna is completely integrated into a cut out of the metal casing.

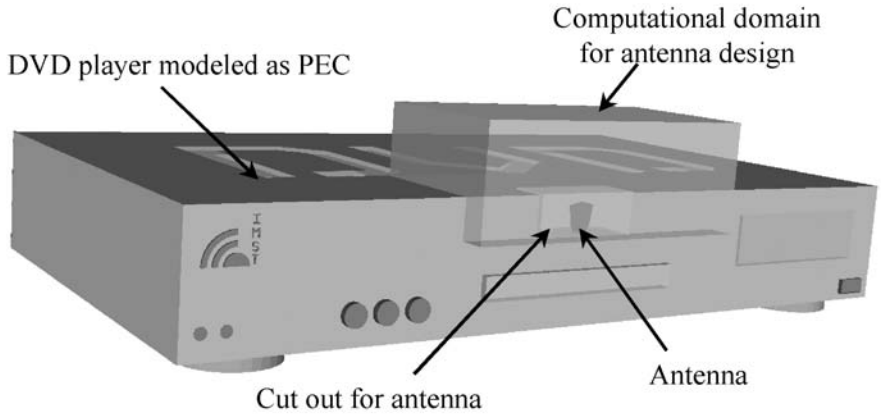

Fig. 7.64. UWB antenna integrated into a numerical model of a DVD player; computational domain used for the antenna design

For the numerical simulation the DVD player is modeled to be a solid PEC (Perfect Electric Conductor). Although this is usually not the case for the original device this can be considered to be a worst-case approximation, on the one hand, and offers certain advantages for the numerical modeling, on the other hand. As already mentioned in Chapter 5, FDTD cells representing a PEC need no direct computation of the field components. They are set to zero. Furthermore, the main influence on the antenna can be foreseen to be the capacitive coupling of the antenna to the metal objects nearby.

The first step of the integration process is to find out the minimum size of this cut out with respect to the antenna matching. In order to generate an efficient simulation model for the fast calculation of only the antenna matching for different sized cut outs, the DVD player is not modeled completely in the first step. If we anticipate that the main influence on the antenna is due to

direct capacitive coupling related only to the size of the cut out, we model first only this part. In Fig. 7.64 the computational domain only consists of the antenna, the cut out and a small portion around. Several metal parts now reach into the PML boundaries and currents excited on the chassis of the DVD player are now absorbed in the PML boundaries. We have to consider that this is in contrast to the realistic case where currents on the chassis can radiate and even get in resonance. When we use this simplified model in the first step, we have to carefully validate the results in a later step by a complete simulation of the whole device. Figure 7.65 shows the matching of the antenna for different sized cut outs.

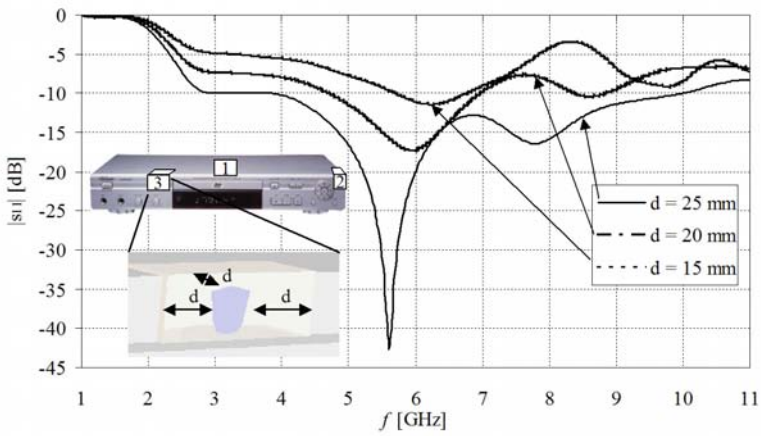

Fig. 7.65. Influence of the size of the cut out on the antenna matching

The investigation shows that the matching of the antenna is still better than 10 dB when the distance to the cut out walls is larger than 25 mm in all dimensions. In a real development case we would now investigate if we could reduce the size of the cut out even more by retuning the antenna element by an optimization of the shape. In this case we are fine with the results as they are. An antenna is not characterized by its matching alone. Another important result is the radiation characteristics. With respect to the nearfield to farfield transformation procedure in Sect. 4.2.7, the farfield cannot be calculated correctly using the above partial simulation model because currents on the chassis would pass through the Huygens surface. Furthermore, these currents on the chassis could affect significantly the radiation pattern. Therefore, in the next step the computational domain will contain the complete DVD player and has a 2 cm distance to the PML walls. The Huygens surface is located around the DVD player in 5 cells distance to the PML boundaries. The overall DVD player is discretized as coarse as possible. If we reduce the maximum excitation frequency to 15 GHz we can use a maximum cell size of

2 mm. We model the entire region outside the small computational domain of Fig. 7.64. All other details that could be identified from the model like switches, volume bottoms, etc. are not refined because it is unlikely that they have significant impact.

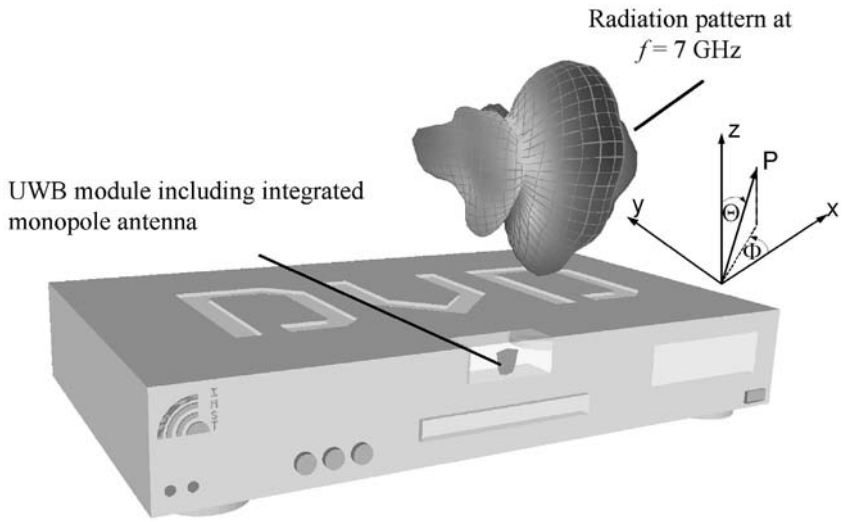

Fig. 7.66. UWB module including an integrated monocone antenna in a DVD player. Calculated radiation pattern at $f = 7$ GHz

Figure 7.66 shows that the radiation pattern of the antenna is significantly affected by the specific integration scenario. While the pattern of the monopole on the groundplane is known to be omnidirectional, the pattern in Fig. 7.66 is clearly directive having significant gain at certain angles and nulls at others.

7.4.4 Establishing an Interface Between Different Modeling Tools for the Entire System Analysis

Assuming that the DVD player is used in a living-room environment for the communication of different home entertainment systems, we could think that the nulls in the radiation pattern may cause problems if another communication module is placed at these angles. On the other hand, we know that in a room we might have a certain level of multipath propagation due to reflection at walls and objects. Therefore it is not obvious to answer the question if we will have sufficient network coverage in a room using the above antenna configuration. To be sure about the entire system performance including the antennas, the channel and the signal processing the computation has to be extended to these items.

http://www.springer.com/978-3-540-28614-1

EM Modeling of Antennas and RF Components for Wireless Communication Systems

Gustrau, F.; Manteuffel, D.

2006, XIX, 276 p., Hardcover
ISBN: 978-3-540-28614-1